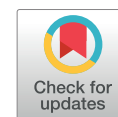


Physics Contribution

# Compartmental Model for $^{223}\text{Ra}$ -Dichloride in Patients With Metastatic Bone Disease From Castration-Resistant Prostate Cancer



Jan Taprogge, PhD,<sup>\*,†,‡</sup> Iain Murray, PhD,<sup>\*,†</sup> Jonathan Gear, PhD,<sup>\*,†</sup>  
Sarah J. Chittenden, BSc. (Hons),<sup>\*,†</sup> Christopher C. Parker, MD,<sup>§</sup>  
and Glenn D. Flux, PhD<sup>\*,†</sup>

*\*Joint Department of Physics, Royal Marsden NHSFT, Sutton, United Kingdom; †The Institute of Cancer Research, London, United Kingdom; ‡Medical Physics and Clinical Engineering, St. George's University Hospital NHSFT, London, United Kingdom; and §Department of Urology, Royal Marsden NHSFT, Sutton, United Kingdom*

Received Mar 19, 2019. Accepted for publication Jul 12, 2019.

## Summary

A better understanding of the uptake mechanisms of  $^{223}\text{Ra}$ -Dichloride is essential for patient-tailored treatment planning and to improve understanding of the effects of alpha radiation on bone tissue. The developed compartmental model suggests that  $^{223}\text{Ra}$ -Dichloride locates on the bone surface and is incorporated into the bone matrix. Those findings could have implications for bone marrow dosimetry and can be used to further investigate the effects of alpha

**Purpose:**  $^{223}\text{Ra}$ -Dichloride is used for treatment of patients with metastatic bone disease from castration-resistant prostate cancer. The uptake and mechanism of action of  $^{223}\text{Ra}$ -Dichloride is not well understood. The aim of this work was to develop a compartmental model for  $^{223}\text{Ra}$ -Dichloride in patients to improve understanding of the underlying mechanisms.

**Methods and Materials:** A compartmental model was developed based on activity retention data from 6 patients (2 treatments of 110 kBq/kg  $^{223}\text{Ra}$ -Dichloride) for plasma, bone surfaces, small intestines, large intestines, and excretion data. Rate constants were extracted. Rate constant variability between patients and treatments was assessed. A population model was proposed and compared with the established International Commission on Radiological Protection-67 compartmental model.

**Results:** A single bone compartment cannot accurately describe activity retention in the skeleton. The addition of a second bone compartment improved the fit to skeleton retention data, and the Akaike information criterion decreased. Mean rate constants of 4.0 (range, 1.9-10.9) and 0.15 (0.07-0.39)  $\text{h}^{-1}$  were obtained for transport from plasma to first bone compartment and vice versa. Rate constants from first to second bone compartment and back of 0.03 (0.02-0.06) and 0.008 (0.003-0.011)  $\text{h}^{-1}$  were calculated. Rate constants for individual patients showed no significant difference between patients and treatments.

Corresponding author: Jan Taprogge, PhD; E-mail: [jan.taprogge@icr.ac.uk](mailto:jan.taprogge@icr.ac.uk)

NHS funding was provided to the NIHR Biomedical Research Centre at The Royal Marsden and the ICR. Data acquisition was funded by Bayer Healthcare Pharmaceuticals and Algeta ASA. The MEDIRAD project has received funding from the Euratom research and training programme 2014-2018 under grant agreement No 755523.

Disclosures: C.P. reports grants and personal fees from Bayer and personal fees from AAA and Janssen, outside the submitted work. J.T.,

I.M., J.G., S.C., and G.F. report grants from Euratom research and training programme 2014-2018, grants from Bayer Healthcare Pharmaceuticals and Algeta ASA for data acquisition, and funding from National Health Service to the NIHR Biomedical Research Centre at The Royal Marsden and the ICR during the conduct of the study.

Supplementary material for this article can be found at <https://doi.org/10.1016/j.ijrobp.2019.07.022>.

radiation on normal bone tissue.

**Conclusions:** The developed compartmental model suggests that  $^{223}\text{Ra}$ -Dichloride initially locates at the bone surface and is then incorporated into the bone matrix relatively quickly. This observation could have implications for dosimetry and understanding of the effects of alpha radiation on normal bone tissue. Results suggest that a population model based on patient measurements is feasible. © 2019 The Author(s). Published by Elsevier Inc. This is an open access article under the CC BY-NC-ND license (<http://creativecommons.org/licenses/by-nc-nd/4.0/>).

## Introduction

$^{223}\text{Ra}$ -Dichloride is used for the treatment of metastatic castration-resistant prostate cancer (mCRPC).<sup>1-4</sup> Skeletal-related events caused by bone metastases are often serious and can reduce the quality of life of patients.<sup>5</sup> Bone-seeking radionuclides such as  $^{32}\text{P}$ -orthophosphate,  $^{89}\text{Sr}$ -chloride, and  $^{153}\text{Sm}$ -EDTMP have been shown to reduce bone pain and have been used to assist in the treatment of bone metastases.<sup>6</sup> The bone marrow absorbed dose is a limiting factor in treatment with beta- and conversion electron-emitting radionuclides.

Alpha emitters have a short range and high linear energy transfer which results in localized energy deposition.<sup>7</sup>  $^{223}\text{Ra}$  is an alpha emitter with a half-life of 11.4 days. The mean path length of the alpha particle emitted by  $^{223}\text{Ra}$  is smaller than 0.1 mm in soft tissue.<sup>5,8</sup> An improvement in overall survival<sup>9,10</sup> and quality of life<sup>11</sup> compared with placebo has been shown when using  $^{223}\text{Ra}$ -Dichloride, although the uptake and mechanism of action of  $^{223}\text{Ra}$ -Dichloride in mCRPC patients is still not well understood.

$^{223}\text{Ra}$ -Dichloride clears quickly from the blood, with only 0.5% remaining 24 hours after administration.<sup>1</sup> Transit from blood to the small intestine (SI) was first shown by Carrasquillo et al<sup>12</sup> with subsequent excretion in feces. Chittenden et al<sup>13</sup> confirmed those findings, with only 1.1% of administered activity remaining in the blood after 24 hours and a large amount (61% at 4 hours) taken up in the skeleton.

Preclinical studies have shown that  $^{223}\text{Ra}$ -Dichloride localizes to bone and is retained.<sup>14,15</sup> Both  $^{223}\text{Ra}$ -Dichloride and  $^{89}\text{Sr}$  concentrate on bone surfaces, and little release of  $^{223}\text{Ra}$ -Dichloride from the bone in the first 14 days after injection was observed. Results from preclinical studies using mouse models provided the first evidence that radium is incorporated into the bone matrix.<sup>16-18</sup> Although it has been suggested that the target of  $^{223}\text{Ra}$ -Dichloride is the hydroxyapatite of newly created bone<sup>19</sup> and radium is often referred to as a calcium analog,<sup>20</sup> to our knowledge no human studies have shown conclusive evidence for this.

Results from clinical trials have shown a lack of hematotoxicity. Hobbs et al<sup>21</sup> developed a bone marrow toxicity model for  $^{223}\text{Ra}$ -Dichloride and concluded that cell level-based dosimetry is necessary to explain the low bone marrow toxicities clinically observed. Moreira et al<sup>22</sup> modelled growth and radiation response of bone metastases and showed that the exposure scenario is essential to

reproduce clinical survival data. They concluded that only a small fraction of cells might be irradiated by  $^{223}\text{Ra}$ . With the limited spatial resolution of planar  $^{223}\text{Ra}$  gamma camera images, it is not feasible to address questions such as the microdistribution of  $^{223}\text{Ra}$ -Dichloride in bone.

Compartmental modeling of the biodistribution and kinetics of  $^{223}\text{Ra}$ -Dichloride can potentially allow the clear limitations of  $^{223}\text{Ra}$  quantitative imaging to be overcome. Available models for radium have only been developed for healthy (reference) humans and animals.<sup>20,23,24</sup> Lassmann et al<sup>25</sup> used the International Commission on Radiological Protection (ICRP) model for radium<sup>23</sup> to calculate absorbed doses for 25 organs and tissues. It remains unclear how the biodistribution is affected in diseased subjects.

The aim of this study was to develop a compartmental model for  $^{223}\text{Ra}$ -Dichloride in patients with mCRPC based on patient data to improve understanding of the underlying mechanisms. Rate constants were determined for each patient and treatment individually to assess inter- and inpatient variability. Results were used to create a population compartmental model for mCRPC patients, based on mean patient rate constants. The model was compared with the ICRP model.<sup>23</sup>

## Methods and Materials

The data set was taken from a phase 1, open-label study (NCT00667537) of the biodistribution, pharmacokinetics, and dosimetry of  $^{223}\text{Ra}$ -Dichloride.<sup>13</sup> Inclusion and exclusion criteria for participation in the study are summarized in Table E1 (available online at <https://doi.org/10.1016/j.ijrobp.2019.07.022>). Informed consent was obtained from all participants in the study, and all procedures performed were in accordance with the ethical standards of the institutional and/or national research committee and with the 1964 Helsinki Declaration and later amendments. Six patients were injected twice (6 weeks apart) with 110 kBq per kg of body mass. Activity retention data were available for blood, plasma, skeleton, SI, upper large intestines (ULI), lower large intestines (LLI), and the whole body.

Activity retained in the blood was measured at 0, 15, 30, and 45 minutes postinjection. Further blood samples were taken at 1, 2, 4, 24, 48, 96, and 144 hours. At each time point, 3 mL of blood was withdrawn using a venous catheter positioned in the arm contralateral to the injection site. A 1 mL whole blood sample, a 1 mL plasma sample, and a 1 mL calibration standard with a known activity

concentration of  $^{223}\text{Ra}$  were measured in an automated gamma counter for 300 seconds per sample to determine whole blood and plasma activity concentrations.

Whole-body measurements were performed using a low-sensitivity scintillation counter comprising a 2" diameter by 2" depth NaI crystal coupled to a photomultiplier tube and preamplifier. The detector, with a lead collimator attached, was fixed at a distance of 2 m above the patient bed. Signal was processed using a PC-based multichannel analyzer with 1024 channels, calibrated to 2 keV per channel. Integral counts obtained for 300 seconds with an 82 keV ( $\pm 20\%$ ) energy window were obtained with the patient lying supine under the detector. Background correction was performed using identical acquisitions without the patient present. A measurement immediately after administration and before any patient voiding was used to convert measured patient counts to injected activity. Optimization of the equipment and methodology for whole-body activity retention measurements was performed according to Chittenden et al.<sup>26</sup> and guidelines published by Hindorf et al.<sup>27</sup> Regular measurements were performed every 2 hours on day 1, and additional (twice per day) readings were taken until the patient was discharged at approximately 48 hours postadministration. Further measurements were performed at 96 and 144 hours postadministration.

Quantitative  $^{223}\text{Ra}$  imaging was performed on a Philips Forte gamma-camera equipped with medium-energy general-purpose collimators according to the protocol outlined by Hindorf et al.<sup>28</sup> A single energy window positioned at 82 keV ( $\pm 20\%$ ) was applied to encompass the 81- and 84-keV transitions of the  $^{223}\text{Ra}$  decay. Planar whole-body images (matrix size  $256 \times 1024$ ) and spot views ( $256 \times 256$ ) were acquired for approximately 30 minutes each. Because of the low counting rate ( $<1$  kilo counts per second), no system dead-time correction was required.

Image quantification was performed by calculating the geometric mean counts of anterior and posterior views using a predetermined sensitivity calibration factor and correcting for patient-specific attenuation. Patient thickness was measured using recent computed tomography scans, and attenuation correction was accomplished based on an effective mass attenuation coefficient according to Hindorf et al.<sup>28</sup> Measurements with a phantom containing spherical inserts were used to estimate sensitivity of the gamma camera.<sup>28</sup>

Retention in the skeleton was extrapolated from activity measurements within regions of interest (ROIs) placed on the skull, left leg, and right leg.  $^{99\text{m}}\text{Tc}$ -MDP scans of the patients were used as a reference to outline bone uptake. Skeletal activity within the torso was not assessed owing to overlying activity within the intestines. Conversion of measured counts to activity per unit mass was performed assuming the masses of the skull and right and left legs from ICRP publication 70.<sup>29</sup> Activity per unit mass was multiplied by the reference mass of the whole skeleton, also taken from ICRP 70, to give the total activity in the skeleton. Additional ROIs around the SI, ULI, and LLI were

used to measure activity within these organs. No specific uptake was seen in kidneys or liver.

Further information on data collection and processing has been described by Chittenden et al.<sup>13</sup> and Hindorf et al.<sup>28</sup> For all organs, the activity retention data are reported here as the fraction of injected activity. Activity concentration in plasma was converted to fraction of injected activity with the assumption of a total plasma volume of 3000 mL.<sup>30</sup> Activity retention data were decay corrected back to the administration time to exclude the physical decay. Two patients were previously identified as super scan patients<sup>13</sup> with widespread skeletal metastases.

## Development of the compartmental model

SAAM II v2.3.<sup>31</sup> was used for compartmental modeling. All rate constants were set to adjustable with lower and higher boundaries of  $0.0001 \text{ h}^{-1}$  and  $1000 \text{ h}^{-1}$ , respectively. Uncertainties for each data point were estimated from the count statistics in the ROIs (SI, LLI, ULI, Skel-eton) and of the blood samples, respectively.

The compartmental model consists of a central plasma compartment, skeleton submodel, and gastrointestinal (GI) submodel with clearance in feces. A rest-of-body compartment was added to account for other organs/tissues not explicitly included in the model (Fig. EA.1; available online at <https://doi.org/10.1016/j.ijrobp.2019.07.022>). Urinary excretion was found to be negligible ( $2 \pm 2\%$  at approximately 48 hours)<sup>13</sup> and was omitted from the model to reduce complexity.

Model development was performed using the forcing function approach. The multicompartamental model was decoupled into 2 separate independent models of the skeleton and the GI tract. In each case, input from a fixed "forcing" function described the activity in the central blood plasma compartment, and an optimal model for each of the submodels was identified. The forcing function was obtained via linear interpolation between sequential plasma activity data points for each patient and treatment individually. Submodels are finally recombined to the full compartmental model.<sup>32,33</sup> Fits of submodels were compared by visual inspection and via the Akaike information criterion (AIC).<sup>34</sup>

For the skeletal activity, submodels with 1, 2, or 3 compartments (Fig. EA.1; available online at <https://doi.org/10.1016/j.ijrobp.2019.07.022>) were fitted to the skeletal activity retention observed for each patient and treatment individually. In the case of submodels with 2 and 3 compartments, the measured skeletal activity retention in patients was taken to be the sum of the activity in the 2 and 3 bone compartments, respectively.

The optimal GI submodel was chosen from submodels with 1 and 3 compartments (Fig. EA.1; available online at <https://doi.org/10.1016/j.ijrobp.2019.07.022>). The single-compartment GI submodel was fitted to the sum of measured activity retention in SI, ULI, and LLI. The

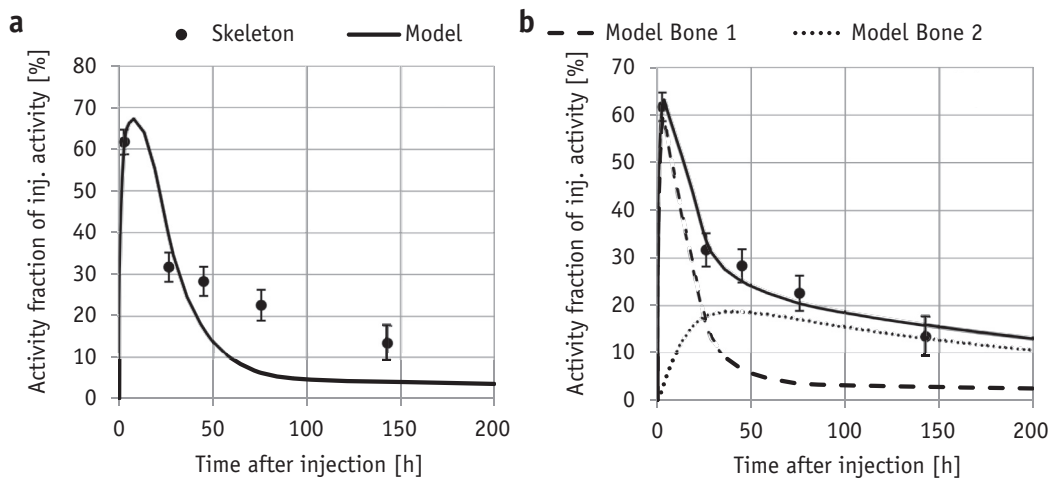


**Fig. 1.** Example for the comparison of fits with (a) a single bone compartment and (b) 2 bone compartments. Circles indicate the skeleton activity retention measurements for the first treatment of patient 4 (P4 T1) as activity fraction of injected activity. The solid line shows the best fit using the submodel with 1 and 2 bone compartments, respectively, while using a forcing function for the plasma compartment. Dashed and dotted lines in (b) represent the model predictions of activity fraction in bone compartment 1 and compartment 2, respectively.

3-compartment submodel was fitted by assigning the measured activity retention in SI, ULI, and LLI to the SI, ULI, and LLI compartments, respectively, for each patient and treatment individually.

Submodels were recombined to form the final structure of the model, and the plasma forcing function was removed. Rate constants from and to the rest-of-body compartment were determined by fitting the model to the full data set including skeleton, SI, ULI, LLI, plasma, and whole-body activity retention per patient and treatment. The full compartmental model was fitted simultaneously to the datasets of activity retention in different organs, and whole-body activity retention was taken to be the sum of all compartments in the body and therefore excluding the feces compartment.

### Inter- and inpatient variability and population model

The set of rate constants for the full compartmental model for each patient and treatment was used to determine inter- and inpatient variability of rate constants. Paired *t* tests were used to identify any significant differences between rate constants of first and second treatments. Paired *t* tests were performed using IBM SPSS v23, and distributions were tested for normality using the Shapiro-Wilk test.

Mean rate constants were calculated, excluding 2 superscan patients, to form the population model. Predicted activity retention in the skeleton was compared with the ICRP 67 model.<sup>23</sup> Skeleton activity retention in the ICRP 67 model was calculated as the sum of the surface compartment, the nonexchangeable volume compartment, and the exchangeable volume compartment for trabecular and cortical bone.

## Results

### The compartmental model

A single-compartment model underestimates the retention in the skeleton at later time points ( $t > 30$  hours) and predicts a faster washout from the skeleton than observed in patients (Fig. 1a). A fit with 2 compartments (Fig. 1b) shows a better agreement (mean AIC, 1.5; range, 0.6-16.6) in comparison to the initial single-compartment model (mean AIC, 40.4; range, 10.8-98.6). The addition of a third compartment did not result in a further fit improvement (mean AIC, 2.5; range, 1.5-18.1). The fits of the remaining skeleton data sets using a 2-compartment skeleton model are shown in Figure 2. Overall a good agreement between fit and activity retention data is found. Notably, the activity retention in patient 3 has a different appearance, most likely because patient 3 is a super-scan patient. Super-scan patients were therefore not included when calculating the population model rate constants.

A 3-compartment model with individual compartments for SI, ULI, and LLI was found to best describe the available data in all patients (Fig. 3). The model is not able to describe the fast uptake into the SI. The AIC of the 3-compartment fit was on average a factor of 19.3 lower compared with the 1-compartment fit.

The final model structure is shown in Figure 4. The predictions of the full compartmental model for activity retention in the different compartments for individual patients were found to be largely consistent with activity retention measured in patients (Fig. EA.2; available online at <https://doi.org/10.1016/j.jrobp.2019.07.022>). Agreement between plasma activity retention model predictions and patient measurements is good (Fig. EA.3; available online at <https://doi.org/10.1016/j.jrobp.2019.07.022>).

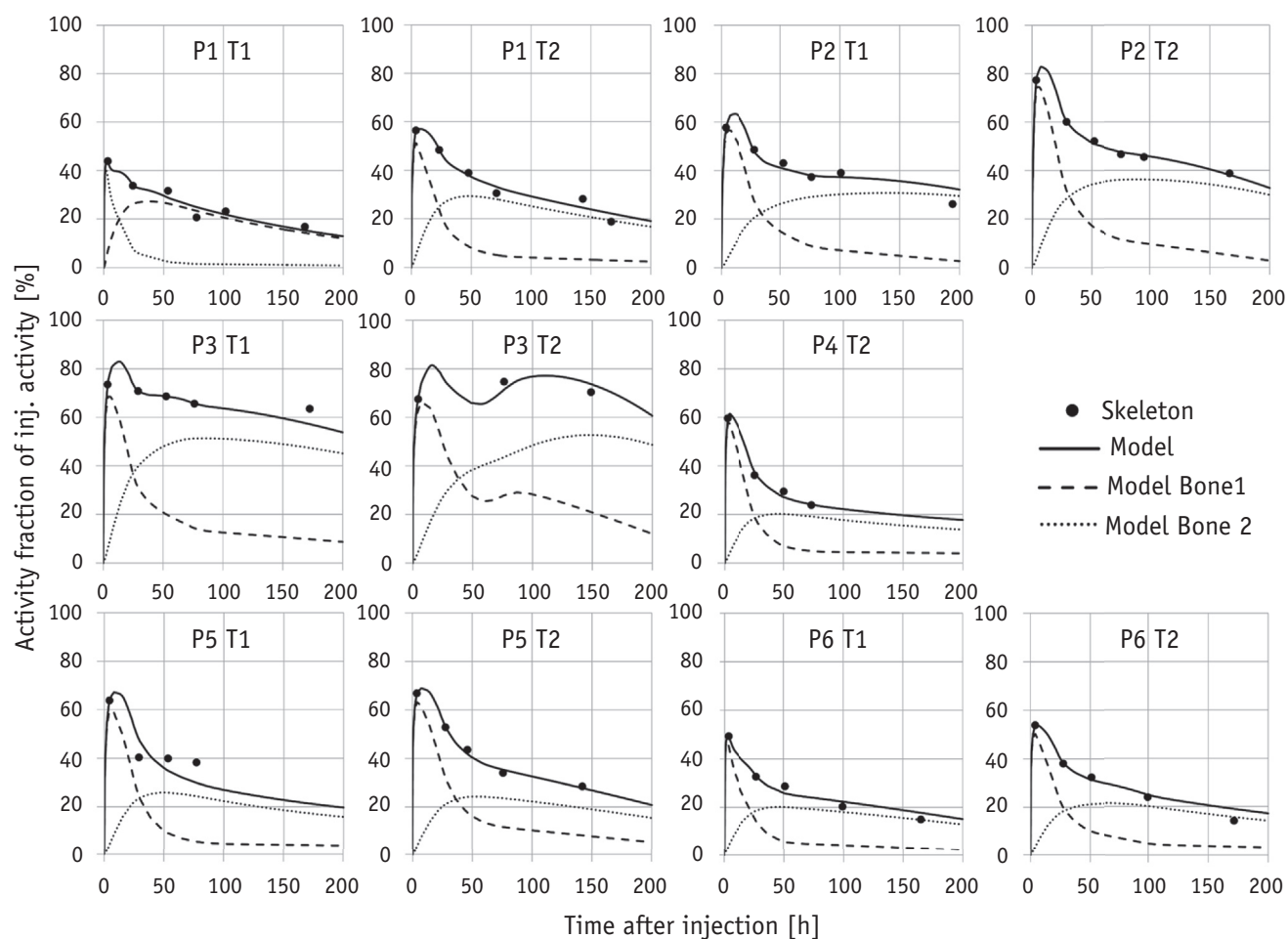


**Fig. 2.** Measured activity fraction in the skeleton of patients is shown as circles. The solid line shows the best fit using the 2 compartment submodel while using a forcing function for the plasma compartment. Dashed and dotted lines represent the model predictions of activity fraction in bone compartment 1 and compartment 2, respectively. The 6 patients are labeled 1 to 6. P1 T1, for example, denotes the first administration for patient 1, and P1 T2 represents the second administration of patient 1.

[doi.org/10.1016/j.ijrobp.2019.07.022](https://doi.org/10.1016/j.ijrobp.2019.07.022)). This indicates that the model complexity is adequate to describe the movement of  $^{223}\text{Ra}$ -Dichloride through the human body.

### Inter and inpatient variability and population model

Rate constants obtained from the individual patient fits are summarized in Table 1. All skeleton submodel and GI submodel rate constants were found to be largely consistent between patients. The coefficient of variation (CoV) of rate constants from and to the second bone compartment ( $k_{B2B1}$  and  $k_{B1B2}$ ) of 25.7% and 44.9% are slightly lower than the CoV of the 2 rate constants from and to plasma ( $k_{B1P}$  and  $k_{PB1}$ ) of 55.1% and 60.4%. CoV of rate constants  $k_{PS}$  and  $k_{SU}$  was found to be 41.8% and 43.9% and was therefore lower than the CoV of rate constants from ULI to LLI and LLI to excretion ( $k_{UL}$  and  $k_{LF}$ ) of 70.3% and 68.0%.

The difference in rate constants  $k_{PB1}$ ,  $k_{B1P}$ ,  $k_{B1B2}$ ,  $k_{B2B1}$ ,  $k_{PS}$ ,  $k_{SU}$ ,  $k_{UL}$ ,  $k_{LF}$ ,  $k_{PR}$ , and  $k_{RP}$  from treatment 1 to

treatment 2 was tested for normality using the Shapiro-Wilk test, and all are approximately normally distributed. Paired *t* tests showed no significant difference between rate constants of the first and the second treatment of patients ( $P > .05$  in all cases).

Rate constants for a population model of  $^{223}\text{Ra}$ -Dichloride in mCRPC patients are presented in Table 1 as well. Comparison of activity retention in the skeleton predicted by the present model and the ICRP model showed that the present model predicts a higher uptake into the skeleton with a significant washout in the first 50 hours (Figure EA.4; available online at <https://doi.org/10.1016/j.ijrobp.2019.07.022>).

### Discussion

The results presented here show that for  $^{223}\text{Ra}$ -Dichloride in mCRPC patients, 2 bone compartments are essential to describe the data. The possibility for 2 or more

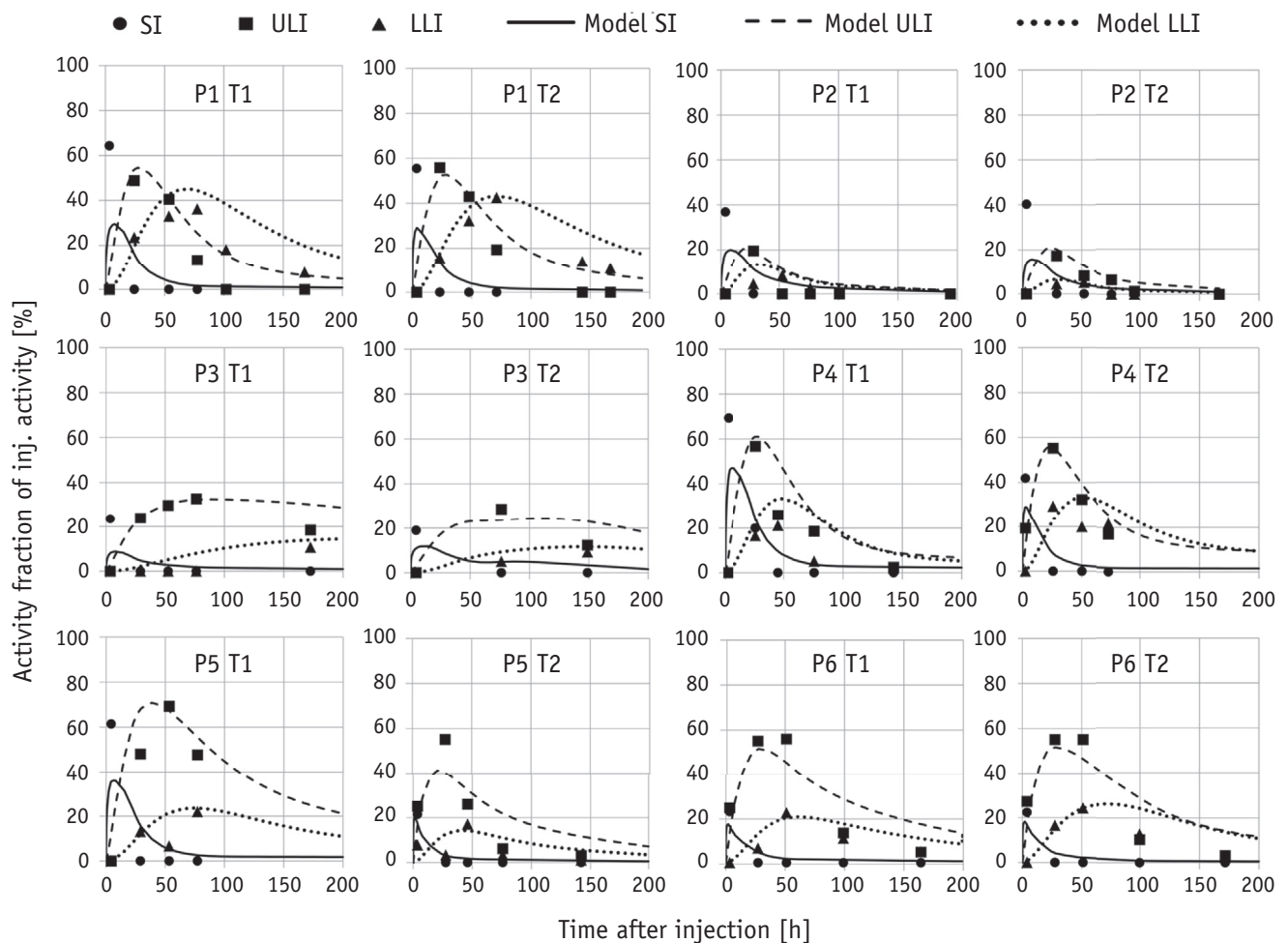


**Fig. 3.** Measured activity fraction of injected activity in the small intestines, upper large intestines, and lower large intestines of patients is shown as circles, squares, and triangles, respectively. The solid, dashed and dotted lines show the best fit for small intestines, upper large intestines, and lower large intestines, respectively, using the 3 compartment submodel while using a forcing function for the plasma compartment.

compartments was already introduced in the ICRP model, where they are described as bone surface and bone volume compartments. The first compartment has a very fast uptake and activity then slowly passes over into the second compartment, which has a very slow release rate. The very different rate constants of the 2 compartments could potentially mean that <sup>223</sup>Ra-Dichloride is found in different locations in the bone.

The uptake and mechanism of action of <sup>223</sup>Ra-Dichloride in mCRPC patients is still not well understood, and only limited preclinical data are available. Preclinical mouse models have shown the first evidence that radium gets incorporated into the bone matrix.<sup>17,18</sup> The similarity between the ICRP and the model developed indicate that these experimental data could be seen as a first indication that <sup>223</sup>Ra-Dichloride is incorporated into the bone matrix in humans.

Initial results from the ERA-223 study (NCT02043678) have shown evidence that a higher fracture rate is observed in patients who have been treated with abiraterone acetate

+ prednisone/prednisole (AAP) and <sup>223</sup>Ra-Dichloride compared with patients treated with AAP and placebo.<sup>3</sup> This increased rate of fractures in the <sup>223</sup>Ra-Dichloride arm of the study is, to date, not well understood, but the European Medicines Agency has subsequently recommended restrictions on the use of <sup>223</sup>Ra-Dichloride.<sup>35</sup> Fractures appeared to have delayed development with respect to treatment with <sup>223</sup>Ra-Dichloride and AAP. Furthermore, fractures typically occurred at sites not involved with bone metastases. Therefore, the model described in this study could form the basis of further work investigating the effect of <sup>223</sup>Ra-Dichloride in normal bone tissue.

Incorporation into the bone matrix also raises questions about the adequacy of bone marrow dosimetry models that do not take into account the exact position of <sup>223</sup>Ra-Dichloride in the bone. <sup>223</sup>Ra has a high linear energy transfer and a very short range in tissue. Dosimetry models that assume a uniform distribution of <sup>223</sup>Ra-Dichloride in the skeleton possibly overestimate the bone marrow

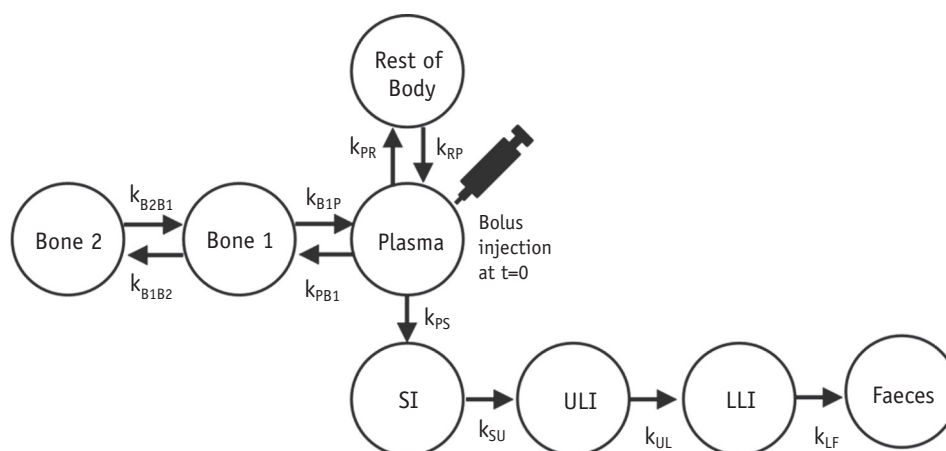


**Fig. 4.** Proposed compartmental model for  $^{223}\text{Ra}$ -Dichloride in patients with metastatic bone disease from castration-resistant prostate cancer in the present study.

toxicity. Hobbs et al.<sup>21</sup> presented results using a marrow cavity model with the activity located on trabecular bone surfaces or endosteal layers. They showed that their model provided markedly different results than standard absorbed fraction calculation. Chittenden et al.<sup>13</sup> hypothesized that marrow toxicity is mainly influenced by the activity circulating in blood and to a lesser extent by the activity on the bone surfaces owing to the short range of the alpha particles. This hypothesis is in agreement with the findings made in the present work, but further investigations are needed to identify the importance of the exact location of  $^{223}\text{Ra}$ -Dichloride on the bone marrow absorbed dose and toxicity, and more data are required. It is hypothesized that the bone marrow absorbed dose from alpha particles in the bone matrix is smaller than from alpha particles located on the bone surface.

Although the present data set and the compartmental model cannot be used to clarify the unknown uptake mechanism, it is clear that this question must be addressed by further clinical studies.

It has been shown that the development of a compartmental model for  $^{223}\text{Ra}$ -Dichloride in patients with mCRPC is feasible and rate constants between treatments and patients are comparable. The limited data set with only 6 patients and 2 treatments is a factor that must be taken into account, and further studies with a larger patient cohort are necessary to improve the population model. Nevertheless, similar pharmacokinetic profiles were observed in the study by Yoshida et al.<sup>36</sup> They showed fast uptake in the bone (52% within 2 hours and maximum uptake was observed within 2 hours of injection). The model proposed here predicts a maximum uptake in the skeleton of 49% at 4 hours. To our knowledge, no studies with larger patient cohorts have collected detailed pharmacokinetic data.

In the current study activity administered was higher compared with the standard clinical dosing of 55 kBq/kg. Nevertheless, results obtained here are expected to be applicable to the standard clinical dosing because the model development does not include any saturation effects and was performed as fraction of injected activity. Yoshida

**Table 1** Mean, minimum, and maximum rate constants from the fits to individual patient data including the 2 superscan patients

Rate constant	Mean of individual patient fits [1/h]	Minimum of individual patient fits [1/h]	Maximum of individual patient fits [1/h]	Population Model [1/h]
$k_{PB1}$	3.990	1.928	10.936	3.041
$k_{B1P}$	0.152	0.071	0.386	0.158
$k_{B1B2}$	0.027	0.017	0.057	0.025
$k_{B2B1}$	0.008	0.003	0.011	0.008
$k_{PS}$	1.423	0.749	2.734	1.519
$k_{SU}$	0.156	0.075	0.257	0.143
$k_{UL}$	0.028	0.006	0.080	0.035
$k_{LF}$	0.040	0.012	0.108	0.047
$k_{PR}$	41.812	4.651	163.276	26.403
$k_{RP}$	5.221	1.387	9.904	5.072

Population model rate constants are excluding the 2 superscan patients. All fits were performed using activity fraction of injected activity decay corrected back to injection time, excluding physical decay.

et al<sup>36</sup> showed that activity retention in the skeleton and plasma are similar in patients injected with 55 kBq/kg and 110 kBq/kg. Furthermore, Carrasquillo et al<sup>12</sup> have shown that plasma pharmacokinetics parameters are comparable for activity levels of 50, 100, and 200 kBq/kg.

The higher initial uptake compared with the ICRP 67 model is an important finding that shows that development of compartmental models using actual patient data is important to verify the use of published models that have been developed for healthy reference, humans, or animals.

## Conclusions

A compartmental model was developed for <sup>223</sup>Ra-Dichloride in mCRPC patients. The model suggests that <sup>223</sup>Ra-Dichloride retention in the human skeleton requires 2 compartments for the bone surface and incorporation into the bone matrix. Further research into the mechanisms of uptake and action of <sup>223</sup>Ra-Dichloride in mCRPC patients is necessary.

## References

1. Nilsson S, Strang P, Aksnes AK, et al. A randomized, dose-response, multicenter phase II study of radium-223 chloride for the palliation of painful bone metastases in patients with castration-resistant prostate cancer. *Eur J Cancer* 2012;48:678-686.
2. Parker C, Nilsson S, Heinrich D, et al. Alpha emitter radium-223 and survival in metastatic prostate cancer. *N Engl J Med* 2013;369:213-223.
3. Smith M, Parker C, Saad F, et al. Addition of radium-223 to abiraterone acetate and prednisone or prednisolone in patients with castration-resistant prostate cancer and bone metastases (ERA 223): A randomised, double-blind, placebo-controlled, phase 3 trial. *Lancet Oncol* 2019;20:408-419.
4. Humm JL, Sartor O, Parker C, et al. Radium-223 in the treatment of osteoblastic metastases: A critical clinical review. *Int J Radiat Oncol Biol Phys* 2015;91:898-906.
5. Attard G, Parker C, Eeles RA, et al. Prostate cancer. *Lancet* 2016;387:70-82.
6. Silberstein EB. Dosage and response in radiopharmaceutical therapy of painful osseous metastases. *J Nucl Med* 1996;37:249-252.
7. Ritter MA, Cleaver JE, Tobias CA. High-LET radiations induce a large proportion of nonrejoining DNA breaks. *Nature* 1977;266:653-655.
8. Florimonte L, Dellavedova L, Maffioli LS. Radium-223 dichloride in clinical practice: A review. *Eur J Nucl Med Mol Imaging* 2016;43:1896-1909.
9. Hoskin P, Sartor O, O'Sullivan JM, et al. Efficacy and safety of radium-223 dichloride in patients with castration-resistant prostate cancer and symptomatic bone metastases, with or without previous docetaxel use: a prespecified subgroup analysis from the randomized, double-blind, phase 3 ALSYMPCA trial. *Lancet Oncol* 2014;15:1397-1406.
10. Sartor O, Coleman R, Nilsson S, et al. Effect of radium-223 dichloride on symptomatic skeletal events in patients with castration-resistant prostate cancer and bone metastases: Results from a phase 3, double-blind, randomised trial. *Lancet Oncol* 2014;15:738-746.
11. Nilsson S, Cislo P, Sartor O, et al. Patient-reported quality-of-life analysis of radium-223 dichloride from the phase III ALSYMPCA study. *Ann Oncol* 2016;27:868-874.
12. Carrasquillo JA, O'Donoghue JA, Pandit-Taskar N, et al. Phase I pharmacokinetic and biodistribution study with escalating doses of <sup>223</sup>Ra-dichloride in men with castration-resistant metastatic prostate cancer. *Eur J Nucl Med Mol Imaging* 2013;40:1384-1393.
13. Chittenden SJ, Hindorf C, Parker CC, et al. A Phase I, Open-Label Study of the Biodistribution, Pharmacokinetics, and Dosimetry of <sup>223</sup>Ra-Dichloride in Patients with Hormone-Refractory Prostate Cancer and Skeletal Metastases. *J Nucl Med* 2015;56:1304-1309.
14. Henriksen G, Breistøl K, Bruland ØS, et al. Significant antitumor effect from bone-seeking, alpha-particle-emitting (<sup>223</sup>Ra) demonstrated in an experimental skeletal metastases model. *Cancer Res* 2002;62:3120-3125.
15. Henriksen G, Fisher DR, Roeske JC, et al. Targeting of osseous sites with alpha-emitting <sup>223</sup>Ra: Comparison with the beta-emitter <sup>89</sup>Sr in mice. *J Nucl Med* 2003;44:252-259.
16. Abou DS, Ulmert D, Doucet M, et al. Whole-body and microenvironmental localization of radium-223 in naive and mouse models of prostate cancer metastasis. *J Natl Cancer Inst* 2015;108:djv380.
17. Suominen MI, Fagerlund KM, Rissanen JP, et al. Radium-223 inhibits osseous prostate cancer growth by dual targeting of cancer cells and bone microenvironment in mouse models. *Clin Cancer Res* 2017;23:4335-4346.
18. Suominen MI, Rissanen JP, Käkönen R, et al. Survival benefit with radium-223 dichloride in a mouse model of breast cancer bone metastasis. *J Natl Cancer Inst* 2013;105:908-916.
19. Sartor O, Hoskin P, Bruland ØS. Targeted radio-nuclide therapy of skeletal metastases. *Cancer Treat Rev* 2013;39:18-26.
20. Leggett RW. A generic age-specific biokinetic model for calcium-like elements. *Radiat Prot Dosimetry* 1992;41:183-198.
21. Hobbs RF, Song H, Watchman CJ, et al. A bone marrow toxicity model for <sup>223</sup>Ra alpha-emitter radiopharmaceutical therapy. *Phys Med Biol* 2012;57:3207-3222.
22. Moreira HMR, Guerra Liberal FDC, O'Sullivan JM, et al. Mechanistic modeling of radium-223 treatment of bone metastases. *Int J Radiat Oncol Biol Phys* 2019;103:1221-1230.
23. ICRP. Age-dependent doses to members of the public from intake of radionuclides - Part 2 ingestion dose coefficients: ICRP Publication 67. *Ann ICRP* 1993;23:95-120.
24. Polig E, Lloyd RD, Bruenger FW, et al. Biokinetic model of radium in humans and beagles. *Health Phys* 2004;86:42-55.
25. Lassmann M, Nosske D. Dosimetry of <sup>223</sup>Ra-chloride: Dose to normal organs and tissues. *Eur J Nucl Med Mol Imaging* 2013;40:207-212.
26. Chittenden SJ, Pratt BE, Pomeroy K, et al. Optimization of Equipment and Methodology for Whole Body Activity Retention Measurements in Children Undergoing Targeted Radionuclide Therapy. *Cancer Biother Radiopharm* 2007;22:243-249.
27. Hindorf C, Glatting G, Chiesa C, et al. EANM Dosimetry Committee guidelines for bone marrow and whole-body dosimetry. *Eur J Nucl Med Mol Imaging* 2010;37:1238-1250.
28. Hindorf C, Chittenden SJ, Aksnes AK, Parker CC, Flux GD. Quantitative imaging of <sup>223</sup>Ra-chloride (Alpharadin) for targeted alpha-emitting radionuclide therapy of bone metastases. *Nucl Med Commun* 2012;33:726-732.
29. ICRP. Basic anatomical and physiological data for use in radiological protection: The skeleton: ICRP Publication 70. *Ann ICRP* 1995;25:1-180.
30. ICRP. Basic anatomical and physiological data for use in radiological protection: Reference values: ICRP Publication 89. *Ann ICRP* 2002;32:1-277.
31. Barrett PHR, Bell BM, Cobelli C, et al. SAAM II: Simulation, analysis, and modeling software for tracer and pharmacokinetic studies. *Metabolism* 1998;47:484-492.
32. Pont F, Duvillard L, Vergès B, et al. Development of compartmental models in stable-isotope experiments. *Arterioscler Thromb Vasc Biol* 1998;18:853-860.
33. Foster DM. Developing and Testing Integrated Multicompartment Models to Describe a Single-Input Multiple-Output Study Using the



- SAAM II Software System. In: Clifford AJ, Müller H-G, editors. *Mathematical Modeling in Experimental Nutrition*. Boston, MA: Springer US; 1998.
34. Akaike H. A new look at the statistical model identification. *IEEE Trans Automat Contr* 1974;19:716-723.
35. European Medicines Agency. Xofigo-H-A-20-1459-C-002653-0028: EPAR – Assessment report – Article 20. EMA/540557/2018. Available at: [https://www.ema.europa.eu/documents/variation-report/xofigo-h-20-1459-c-002653-0028-epar-assessment-report-article-20\\_en.pdf](https://www.ema.europa.eu/documents/variation-report/xofigo-h-20-1459-c-002653-0028-epar-assessment-report-article-20_en.pdf). Accessed April 2, 2018.
36. Yoshida K, Kaneta T, Takano S, et al. Pharmacokinetics of single dose radium-223 dichloride (BAY 88-8223) in Japanese patients with castration-resistant prostate cancer and bone metastases. *Ann Nucl Med* 2016;30:453-460.